JOURNAL OF MATERIALS SCIENCE **39** (2004) 2821–2826

Hydrothermal synthesis of $LaMnO_{3+\delta}$: F.T.I.R. and W.A.X.S. investigations of the evolution from amorphous to crystallized powder

C. BERNARD, B. DURAND*
Centre Interuniversitaire de Recherche et d'Ingénierie des Matériaux, CNRS-UMR 5085, Université Paul Sabatier, 118 Route de Narbonne, 31062 Toulouse Cedex 04, France
E-mail: bdurand@chimie.ups-tlse.fr

M. VERELST, P. LECANTE
Centre Elaboration des Matériaux et d'Etudes Structurales, 29 rue Jeanne Marvig, BP4347, 31055 Toulouse Cedex 04, France

Pseudo-cubic $LaMnO_{3+\delta}$ powders were obtained by pyrolysis of the amorphous residue of the hydrothermal treatment, at 150°C under autogeneous pressure, of lanthanum and manganese nitrates in presence of citric acid. The pyrolysis steps are identified by coupled T.G.A.-D.T.A. determining also the carbon content evolution. From F.T.I.R. and W.A.X.S. investigation of the amorphous powders calcined at various temperatures in the 200–1000°C range, it is shown that the crystallization occurs slowly in the 550–700°C range and that the perovskite skeleton already exists in the amorphous citrate precursors formed by the hydrothermal treatment.

1. Introduction

Manganese oxides $A_{1-x}B_xMnO_3$ (A = trivalent rare-earth; B = divalent metal such as Ca, Sr, Ba, or Pb) crystallizing in a perovskite type structure generate great interest because of their various electronic, magnetic and structural properties, and the related potential applications [1, 2]. Their magnetic structure and electronic transport properties are correlated via the hopping of electrons between Mn^{3+} and Mn^{4+} ions and the presence of cationic vacancies. But these perovskite oxides also display prominent catalytic activity in many reactions [3, 4], including total oxidation of hydrocarbons and volatile organic compounds [5, 6]. Their use in this field of catalysis appears very promising, since they could lead to cheaper materials by the substitution of noble metals supported on alumina, silica or other inert solids.

Various methods can be used for the synthesis of lanthanum manganite $LaMnO_{3+\delta}$ including conventional solid-state reaction [7], coprecipitation [8–10], sol gel [11] and molten salts reactions [12]. Concerning hydrothermal synthesis, the literature is scarce. Ovenstone and Ponton [13] reported the preparation of lanthanum manganite mainly from acetate precursors in hydrothermal media adjusted at basic pH by ammonium hydroxide or organic bases (TMAH, TEAH). We reinvestigated the hydrothermal synthesis of manganites $La_{1-x}Sr_xMnO_{3+\delta}$ with special interest for the influence of synthesis parameters, particularly that of complexing agents, such as citric acid [14]. Our conclusions are similar to those of Ovenstone and Ponton:

(i) the hydrothermal treatment never leads directly to crystallized $LaMnO_{3+\delta}$

(ii) when the residue of the hydrothermal treatement is a mixture of crystallized $La(OH)_3$ and Mn_3O_4, its annealing at 1000°C for 2 h leads to crystallized $LaMnO_{3+\delta}$ only when the hydrothermal reaction is carried out in very narrow ranges of temperature and time.

(iii) when the residue of the hydrothermal treatement is an amorphous solid, the crystallization of $LaMnO_{3+\delta}$ occurs as soon as 650°C and the hydrothermal treatment can be performed in wide ranges of temperature and time.

The present paper deals with the analysis, by F.T.I.R and W.A.X.S. of the transformation of the amorphous powder into crystallized $LaMnO_{3+\delta}$, when the hydrothermal synthesis is performed in presence of citric acid.

2. Experimental

2.1. Preparation of amorphous powders

The amorphous precursors of lanthanum manganite $LaMnO_{3+\delta}$ were prepared by hydrothermal treatment, at 150°C for 20 h under autogenous pressure, of aqueous media containing $La(NO_3)_3$-$5.5H_2O$, $Mn(NO_3)_2$-$6H_2O$, citric acid and ammonia for pH adjustment. The procedure and the characteristics of the manganite formed by pyrolysis at 650°C have been published previously [14].

* Author to whom all correspondence should be addressed.

2.2. Investigation of the pyrolysis step

The amorphous precursor was calcined in air at the following temperatures: 200, 300, 400, 500, 550, 600, 650, 700, 900 and 1000°C. The pyrolysis was carried out by heating at a rate of $100°C \cdot h^{-1}$ and maintaining 2 h dwell at the chosen temperature.

Infrared spectroscopy (F.T.I.R.) was performed using a Perkin Elmer 1760X Fourier Transformed Infrared spectrometer equipped with a TGS detector. Samples were incorporated in KBr pellets (2 mg of sample for 200 mg of KBr); 128 scans were recorded and the resolution of spectra was estimated to be 4 cm^{-1}.

Due to poor compound crystallinity, classical powder X-ray diffraction (X.R.D.) was unable to give accurate crystallographic data. Hence, structural investigations were performed using a Philips PF 1380 diffractometer modified in the C.E.M.E.S. laboratory so as to work in wide angle X-ray scattering (W.A.X.S.) mode according to the following procedure. The sample was sealed in a Lindeman capillary and the diffraction pattern was obtained by irradiating the sample with graphite-monochromatized Mo K_α radiation ($\lambda = 0.71069$ Å). 457 intensities corresponding to equidistant 's' points ($s = 4\pi \sin\theta/\lambda$; $\delta s = 0.035$ $Å^{-1}$) were collected in the range $0 < \theta < 65°$. A blank run was also done with an empty capillary under the same conditions. The raw sample scattered intensity (sample + air + capillary) was corrected, for air and capillary contribution, by spectral subtraction taking into account the absorption of the sample, and then corrected for polarization and self absorption effects. Normalization was performed using the Norman and Krogh-Moe's [15, 16] method. The atomic scattering factors were taken from Cromer and Waber [17]. The interatomic distances in direct space were calculated from the experimentally reduced radial distribution function (R.D.F.), following the same procedure than for earlier studies [18–21]. W.A.X.S. data were collected using a classic computer-controlled two-circles diffractometer optimized to get a low instrument background: air and other parasitic scatterings are reduced by the combination of short air pathlenght and long slits. On the other hand, a graphite monochromator and large aperture provide high intensity with the trade off of a low spatial resolution, however not required since nanocrystalline compounds by principle don't exhibit sharp peaks. For the better crystallized sample annealed at 650°C, a direct comparison with the International Center for Diffraction Data (I.C.D.D.) file was also performed.

The carbon content of each sample was determined, by chemical analysis, in the C.N.R.S. Microanalysis Center of Vernaison by induced coupled plasma (I.C.P.)

The specific surface area of powders was estimated by nitrogen adsorption-desorption according to the B.E.T. method with a Micromeritics Desorb 2300 A porosimeter; samples were outgassed at 150°C.

Coupled thermogravimetric-thermodifferential analyses (T.G.A.-D.T.A.) were performed on a Setaram 92 analyser working under air flow ($0.8\ L \cdot h^{-1}$) at a rate of $5°C \cdot min^{-1}$.

3. Results

3.1. F.T.I.R. spectroscopy

In the 1200–900 cm^{-1} wave number range, the F.T.I.R. spectra of samples as prepared (150°C) and calcined at 400°C show a strong evolution (Fig. 1). The former spectrum exhibits five bands all characteristic of vibrations of citric anions [12]. These bands disappear after calcination and the latter spectrum shows only one broad band centered around 1071 cm^{-1} and attributed to a ν_s(COO) vibration of the carbonate anion CO_3^{2-}. According to Gajbkinye [23], the decomposition of nickel iron citrate occurs between 200 and 320°C.

In the 1800–1200 cm^{-1} wave number range, the F.T.I.R. spectra of samples annealed at 500, 550, 600 and 700°C (Fig. 2a) reveal two broad bands centered around 1481 and 1396 cm^{-1}, with amplitudes decreasing when the annealing temperature increases; they are attributed to CO_3^{2-} anion vibrations (ν_{as} (COO)). A narrow band pointing at 1380 cm^{-1} is assigned to the NO_3^- anions. It also vanishes when the annealing temperature increases; this proves that the washing of powders does not completely remove NO_3^- anions coming from the metal precursors. In the 1000–400 cm^{-1} wave number range, the F.T.I.R. spectra show the formation of a strong band at 610 cm^{-1} typical of Me—O bonds in perovskite structure (Fig. 2b). It appears at 550°C and its amplitude increases with annealing temperature. A last medium band at 850 cm^{-1}, whose amplitude quickly decreases as the annealing temperature is raised, is assigned to ν_s (COO). The carbonate groups remaining after calcination at 700°C are probably surface carbonates. Indeed, the same bands are observed on the F.T.I.R. spectrum of lanthanum oxide prepared by calcination in air of lanthanum nitrate. Therefore, it is shown that the crystallization of the perovskite phase begins at 550°C

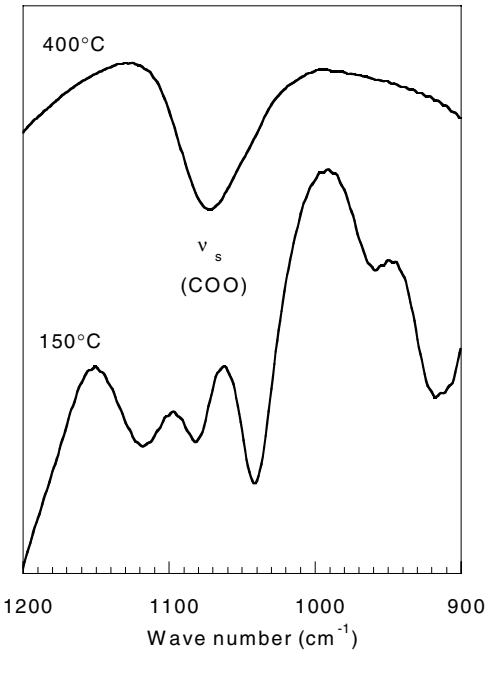

Figure 1 F.T.I.R. spectra of the as-prepared amorphous powder (150°C) and of the powder annealed at 400°C.

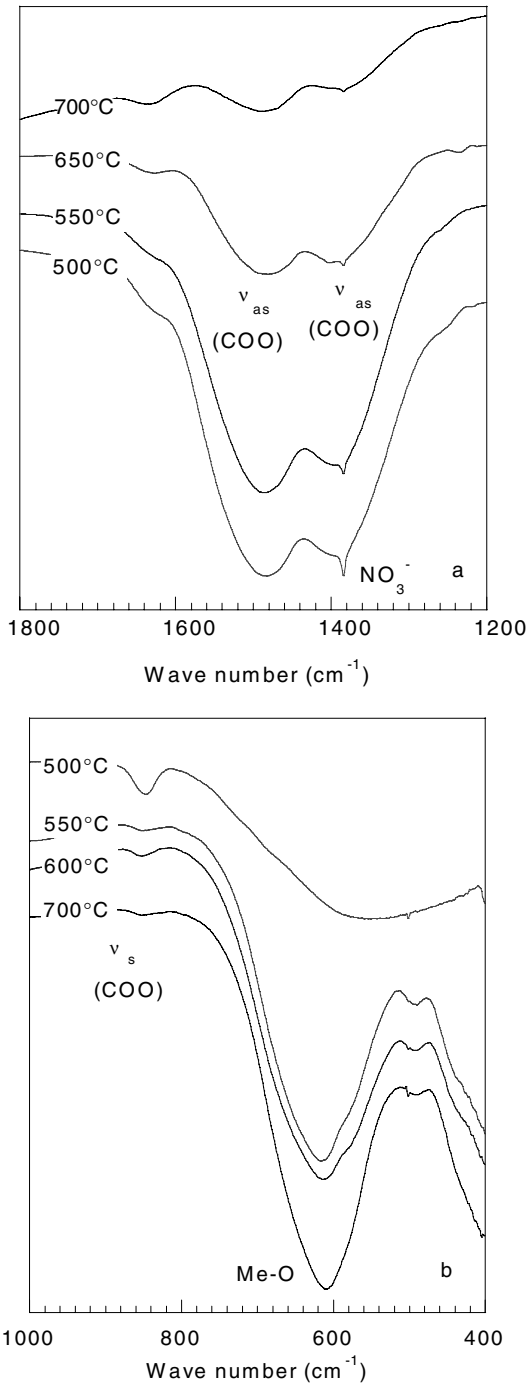

Figure 2 Influence of the increase of annealing temperature on the F.T.I.R. spectra of powders: in the wave number range 1800–1200 cm^{-1} (a) and 1000–400 cm^{-1} (b).

and is finished at 700°C. Crystallization starting temperature, evidenced from I.R. spectroscopy, is about a hundred degrees lower than that determined by X.R.D. at variable temperatures [14].

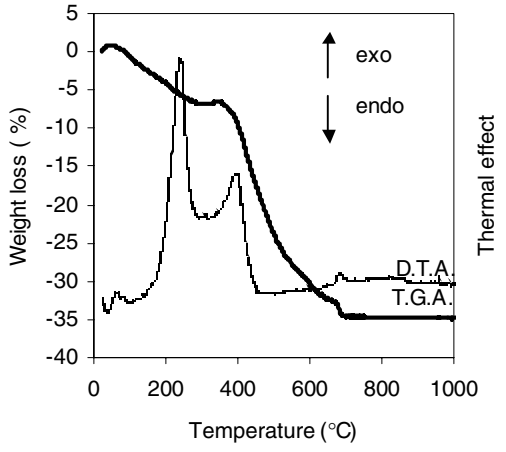

Figure 3 T.G.A. and D.T.A. plots of the as-prepared amorphous powder.

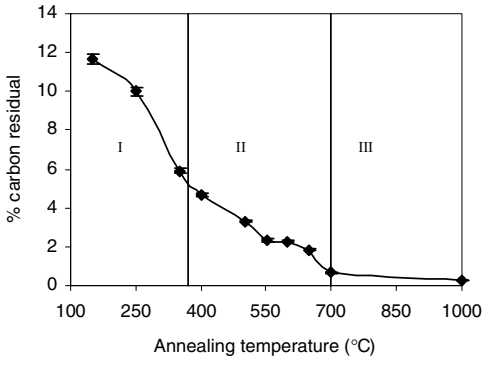

Figure 4 Influence of the annealing temperature on the carbon content of samples.

3.2. Thermal analysis and carbon content determination

The thermal analysis (coupled D.T.A-T.G.A) reveals a multistep pyrolysis (Fig. 3). The data and their interpretation are summarized in Table I.

The study of the pyrolysis by the determination of the carbon content of the calcined samples (Fig. 4) shows that the carbon loss kinetics are more significant for the transformation of citrate into carbonate (area I) than for the transformation of carbonate into oxide (area II). The crystallization of $LaMnO_{3+\delta}$ also occurs with a carbon loss.

The specific surface area is not significantly affected by the transformations occurring in the amorphous powder before crystallization. A regular decrease is then observed for the samples calcined above crystallization temperature (Table II).

3.3. Structural analysis: WAXS

Analysis has been performed on a non annealed sample (150°C) and annealed ones up to 650°C. Beyond

TABLE I Interpretation of T.G.A-D.T.A. data

T.G.A.		D.T.A.		
T range (°C)	Weight loss (%)	Thermal effect	*T* (°C)	Interpretation
Ambient-140	2.5	Not clearly identified		Dehydration
140–350	6.5	Exo	240	Citrate species decomposition
350–650	26.5	Exo	395	Carbonate species decomposition
650–700	2	Exo	680	$LaMnO_{3+\delta}$ crystallization

TABLE II Influence of annealing temperature on the specific surface area of powder (S_w)

Annealing temperature (°C)	150	200	300	400	500	550	600	650	700	800	900	1000
S_w ($m^2 \cdot g^{-1}$)	28	28	32	30	25	23	27	28	26	14	9	6

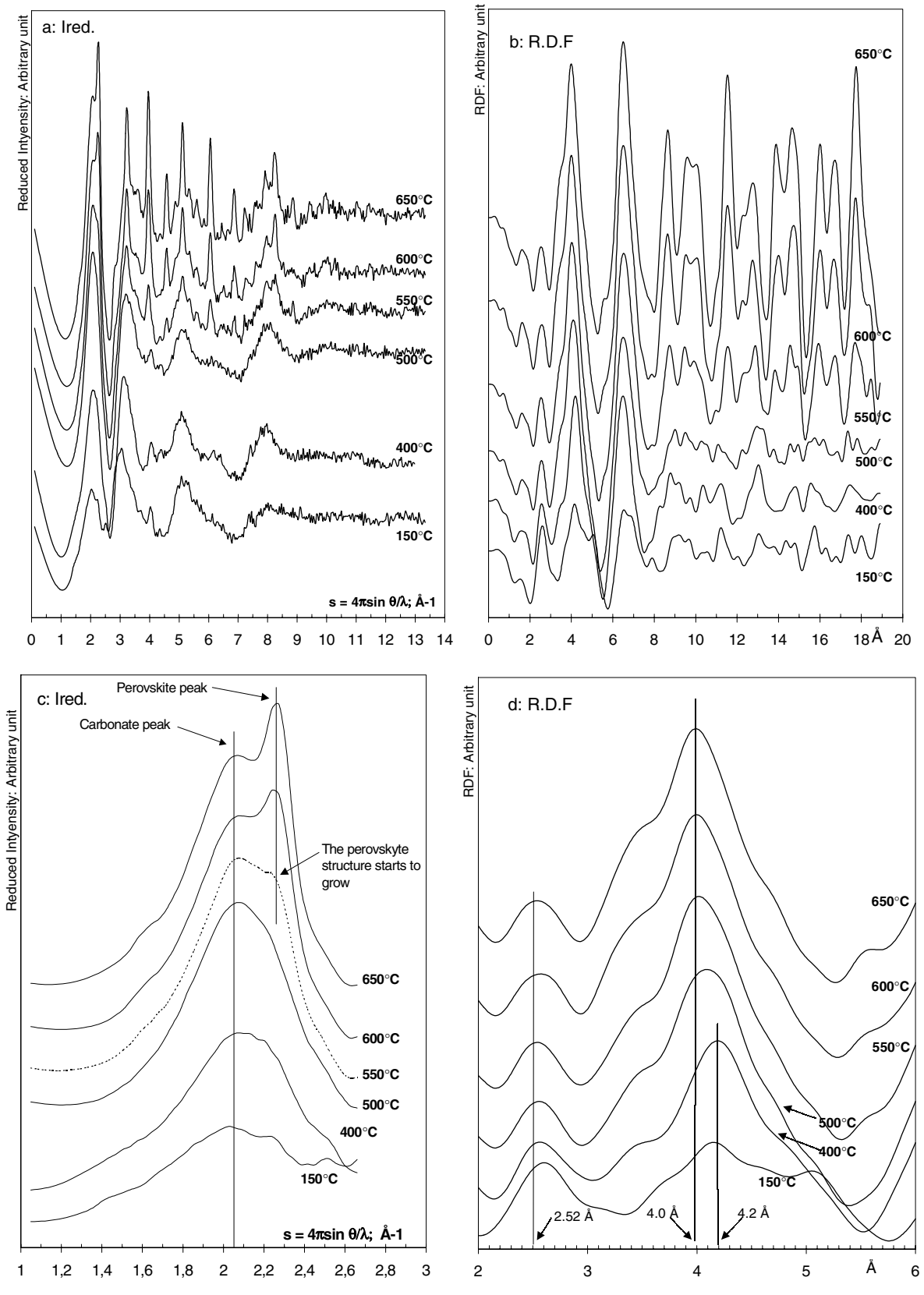

Figure 5 WAXS analysis: influence of the increase of annealing temperature on the plots of reduced intensity (reciprocal space) (a) and radial distribution function (direct space) (b) for the full pattern; zooming into the area 1–3 $Å^{-1}$ for the reduced intensity plot (c) and into the area 2–6 Å for the R.D.F. plot (d).

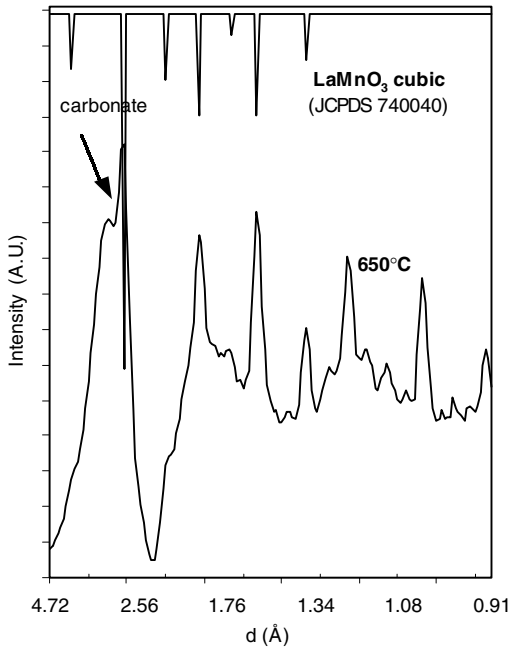

Figure 6 Comparison between the scattered intensity versus d ($d = \lambda/2{\cdot}\sin\theta$) for the sample annealed at 650°C and the J.C.P.D.S. file reported for cubic $LaMnO_3$.

this value (700°C), the compound becomes a pure $LaMnO_{3+\delta}$ well crystallized phase which can be studied using classical XRD. Fig. 5a and b show respectively the reduced intensity (Ired) and the radial distribution function (R.D.F.) for each sample. The reduced intensity represents the structural part of the scattering phenomenon after the full correction procedure. The Fourier transform of this spectrum gives the R.D.F which can be considered as a histogram of ordered distances weighted by the distance multiplicity and the number of electrons engaged in these bonds. Thus, an intense peak on the R.D.F. indicates a very frequent distance between two heavy atoms. Fig. 5c and d display finer scale details of the 1–3 $Å^{-1}$ range in the reciprocal space (Ired) and the 2–6 Å range in the real space.

From 150 to 650°C, a gradual increase of the crystallinity of the compounds can be observed, on both reduced intensity and R.D.F. curves.

Even at 650°C, an amorphous phase remains the major component. According to I.R. spectroscopy, we can reasonably postulate that this amorphous phase is a carbonate or oxycarbonate compound.

At 550°C, well defined crystalline peaks start to grow from the amorphous shoulders, but clearly the kinetics of this evolution are slow since at 650°C the amorphous "carbonate" contribution remains. The crystallinity is however sufficient to compare the diffuse/diffracted pattern with I.C.D.D. files (Fig. 6) at 650°C. Clearly the crystallized phase which is forming above 550°C is a perovskite structure. However, one notes that, although the selected perovskite file is that of the cubic phase, the structure of the sample annealed at 650°C is not necessarily cubic. Indeed, for such broad peaks, a weak distorsion on the X.R.D. patterns (peak splitting), corresponding to a rhombohedral or orthorhombic distorsion, could not be evidenced but remains possible.

More definitive conclusions, can be extracted from the zoomed zones shown on Fig. 5d. The first shoulder centered at 2.52 Å represents the average contribution of La─O (∼2.70 Å) and Mn─O (∼2.20 Å) nearest pair distances. This peak does not evolve from 150 to 650°C which indicates that the coordination sphere around La and Mn does not change much between these two temperatures. More interesting is the evolution of the peak centered at 4.2 Å. For the perovskite structure, this corresponds to the unit cell parameter, including both the La─La and Mn─Mn pair distances (light element interaction can be neglected since the X-ray scattering phenomenon is strongly dominated by heavy atoms). So, the main difference between the carbonate and the perovskite structure is this metal-metal distance which suddently drops from 4.2 Å for the carbonate compounds down to 4.0 Å for the perovskite structure. However, it has to be noted that this value of 4.0 Å is an average contribution between the perovskite structure itself ($a = 3.883$ Å) and the remaining carbonates still present at 650°C.

4. Conclusion

From this structural study, we can assert that the final perovskite (La,Mn)-O-(La,Mn) skeleton is already in place, albeit roughly, in the citrate precursor and does not significantly change during the thermal treatments. Of course, that does not mean that the citrate precursor or carbonate intermediate already has a perovskite structure at this stage but simply that a metal-oxygen 3D network is present in the precursors and that the de-carbonatation phenomenon does not interfere with this.

Acknowledgment

The authors are grateful to Marie Thérèse BOISDON and Chantal ANDRE for infra red spectroscopy.

References

1. R. VON HELMOLT, J. WECKER, B. HOLZAPFEL, L. SCHULTZ and K. SAMWER, *Phys. Rev. Lett.* **71** (1993) 2331.
2. J. M. D. COEY, M. VIRET and S. VON MOLNAR, *Adv. Phys.* **48** (1999) 167.
3. A. HAMMOUCHE, E. SIEBERT, A. HAMMOU and M. KLEITZ, *J. Electrochem. Soc.* **138**(5) (1991) 1212.
4. M. F. ZWINKELS, S. G. JARAS and P. G. MENON, *Catal. Rev. Sci. Eng.* **35** (1993) 319.
5. A. MUSIALIK-PIOTROWSKA and K. SYCZEWSKA, *Catal. Today* **59** (2000) 269.
6. T. SEIYAMA, *Catal. Rev. Sci. Eng.* **34** (1992) 281.
7. A. A. BARRESI, S. RONCHETTI, M. BENGL, D. MAZZA and G. BALDI, *Proc. IcheaP-4, Firenze* **1**(27) (1999) 572.
8. M. CRESPIN and W. K. HALL, *J. Catal.* **69** (1981) 359.
9. A. M. DUPRAT, PhD thesis, Thèse de Doctorat of the University of Toulouse, 1995, no d'ordre 1968, p. 30.
10. I. MAURIN, P. BARBOUX, Y. LASSAILLY and J. P. BOILOT, *Chem. Mater.* **10** (1998) 1727.
11. S. BULGEZ, E. SYSKAKIS, A. NAOUMIDIS and H. NICKEL, *J. Amer. Ceram. Soc.* **75** (1992) 964.
12. C. CIARAVINO, R. LYONNET, J. P. SCHARFF, B. DURAND and J. P. DELOUME, *J. High. Temp. Mater. Proc.* **3**(2) (1999) 269.

13. J. OVENSTON and C. B. PONTON, *Brit. Ceram. Proc.* **0**(58) (1998) 155.
14. C. BERNARD, C. LABERTY, F. ANSART and B. DURAND, *Ann. Chim. Sci. Mater.* **5** (2003) 85.
15. N. J. NORMAN, *Acta Crystallogr.* **10** (1957) 370.
16. J. KROGH-MOE, *ibid.* **9** (1956) 951.
17. D. CROMER and J. WABER, "International Tables for X-ray Crystallography" (Kynoch Press, Birmingham, 1974) Vol. 4.
18. T. VOGT, C. FAULMANN, R. SOULES, P. LECANTE, A. MOSSET, P. CASTAN, P. CASSOUX and J. GALY, *J. Amer. Chem. Soc.* **110** (1988) 1833.
19. C. LABERY, M. VERELST, P. LECANTE, A. MOSSET, P. ALPHONSE and A. ROUSSET, *J. Solid State Chem.* **129** (1997) 271.
20. S. MEGE, M. VERELST, P. LECANTE, E. PEREZ, F. ANSART and J. M. SAVARIAULT, *J. Non-Cryst. Solids* **283** (1998) 37.
21. P. ELUMALAI, H. N. VASAN, M. VERELST, P. LECANTE, V. CARLES and P. TAILHADES, *Mater. Res. Bull.* **37** (2002) 353.
22. B. SCHRADER, "Raman/Infrared Atlas of Organic Compounds," 2nd ed. (VCH, 1999) p. B3-14.
23. N. S. GAJBKINYE and S. PRASAD, *Thermochimica Acta* **285**(2) (1996) 325.

Received 20 December 2002
and accepted 23 December 2003